Current Research in Food Science 8 (2024) 100749

Contents lists available at ScienceDirect

Current Research in Food Science

journal homepage: www.sciencedirect.com/journal/current-research-in-food-science

Effect and potential mechanism of nitrite reductase B on nitrite degradation by *Limosilactobacillus fermentum* RC4

Qing Fan [a,b,c,1], Chaoran Xia [a,b,c,1], Xiaoqun Zeng [a,b,c,*], Zhen Wu [a,b,c], Yuxing Guo [a,d], Qiwei Du [a,b,c], Maolin Tu [a,b,c], Xinanbei Liu [e], Daodong Pan [a,b,c]

[a] State Key Laboratory for Managing Biotic and Chemical Threats to the Quality and Safety of Agro-products, Ningbo University, Ningbo, China
[b] Key Laboratory of Animal Protein Food Processing Technology of Zhejiang Province, College of Food Science and Engineering, Ningbo University, Ningbo, China
[c] Zhejiang-Malaysia Joint Research Laboratory for Agricultural Product Processing and Nutrition, Ningbo University, Ningbo, China
[d] School of Food Science and Pharmaceutical Engineering, Nanjing Normal University, Nanjing, China
[e] College of Resources and Environment, Baoshan University, Baoshan, China

ARTICLE INFO

Handling Editor: Dr. Siyun Wang

Keywords:
Nitrite degradation
Nitrite reductase
*nir*B gene
Limosilactobacillus fermentum RC4
Whole-genome sequence

ABSTRACT

Nitrite has the potential risk of hypoxic poisoning or cancer in pickled food. In our previous study, *Limosilactobacillus fermentum* (*L. fermentum*) RC4 is effective in nitrite degradation by producing nitrite reductase B (NirB). To investigate the detailed mechanism from the genome, response, and regulation of NirB, the whole-genome sequence of *L. fermentum* RC4 was analyzed, the *L. fermentum*-EGFP-*nir*B with enhanced green fluorescent protein (EGFP) labeled the nitrite reductase large subunit *nir*B, and the recombined *L. fermentum*-NirB with overexpression NirB strain was conducted. The key genes within the dominant metabolism pathways may be involved in stress tolerance to regulate the degrading process. The green fluorescence density of EGFP indicated that NirB activity has a threshold and peaked under 300 mg/L nitrite concentration. NirB overexpressed in *L. fermentum* RC4 boosted the enzyme activity by 39.6% and the degradation rate by 10.5%, when fermented in 300 mg/L for 40 h, compared to the control group. RNA-seq detected 248 differential genes mainly enriched in carbohydrate, amino acid, and energy metabolism. The *ack*A gene for pyruvate metabolism and the *mtn*N gene for cysteine metabolism were up-regulated. NirB regulates these genes to produce acid and improve stress resistance for *L. fermentum* RC4 to accelerate nitrite degradation.

1. Introduction

Nitrite primarily exists in the form of sodium nitrite ($NaNO_2$) in cured products. In addition to the externally added nitrite during the curing process, nitrogen-containing compounds are converted into nitrite under the amination and nitrification of endogenous microbiota (Giguere et al., 2018). Nitrite is frequently used to improve food quality, for example, making meat products bright red in color (Huang et al., 2019), inhibiting the growth and metabolism of pathogenic bacteria (Elias et al., 2020), preventing lipid peroxidation and reduce the generation of bad smell in pickled food (Duan et al., 2018). The residual nitrite interacts with amine or amide substances in the human body to produce strong carcinogenic N-nitrosamine compounds raise cancer risks (Chetty et al., 2018), and oxidize human hemoglobin reducing the capacity of oxygen delivery (Stepuro et al., 2012).

Lactic acid bacteria (LAB), as the predominant food-grade probiotic in fermented and pickled foods, possess a unique enzyme system capable of reducing nitrosamine and controlling endotoxin, enabling them to produce nitrite reductase to degrade nitrite (Yu and Zhang, 2013). Nitrite degradation by LAB includes enzymatic degradation, acidic degradation, and produces non-acid and non-enzymatic substances (Xia et al., 2022). In the early stage of fermentation, LAB produces less acid and a small amount of H^+ neutralizes nitrite reductase acting on nitrogen oxides (Hu et al., 2023). In the later stage of fermentation, the non-enzyme disproportionation reaction between nitrite and a large amount of H^+ generated by LAB causes NO_2^- to be transformed into NO inhibiting the activity of nitrite reductase (Tiso and Schechter, 2015). Besides, the nisin (dos Santos et al., 2023), exopolysaccharide (Zhu

* Corresponding author. Key Laboratory of Animal Protein Food Processing Technology of Zhejiang Province, College of Food Science and Engineering, Ningbo University, Ningbo, 315800, China.
E-mail address: zengxiaoqun@nbu.edu.cn (X. Zeng).
[1] Theses authors contributed equally to this work.

https://doi.org/10.1016/j.crfs.2024.100749
Received 29 November 2023; Received in revised form 22 April 2024; Accepted 22 April 2024
Available online 24 April 2024

et al., 2018), vitamin (Du et al., 2018), and protein compound (Fang et al., 2016) produced by LAB showed well nitrite depletion ability in sausages and pickles.

Nitrite reductase, an intracellular enzyme that exists in the cytoplasm as well as in the periplasm space or cell membrane, can reduce nitrite to NO or NH_3 in the nitrogen cycle (Khlebodarova et al., 2016). Based on the difference in reactants and cofactors, nitrite reductases can be divided into Cu-containing nitrite reductase (CuNiRs), cytochrome cd_1 nitrite reductase (cd_1NiRs), cytochrome *c* nitrite reductase (ccNiRs) and ferredoxin-dependent nitrite reductase (FdNiRs) (Gao et al., 2017). Nitrite reductase B (NirB), an enzyme involved in the nitrogen cycle ammonification pathway, employs NADH as an electron donor to decrease nitrite in the cytoplasm under anaerobic conditions. The large subunit NirB and the small subunit NirD, encoded by the *nir*B and *nir*D genes respectively, work together to degrade nitrite by forming the NirBD complex. The two iron–sulfur clusters (4Fe-4S) of NirB control the electron transport and nitrite reduction (Izumi et al., 2012).

In previous work, isobaric tags for relative and absolute quantification (iTRAQ) proteomics and bioinformatics analysis were used to investigate the protein expression patterns of nitrite degradation by *L. fermentum* RC4. Enzymatic degradation is dominating, and the expression of key gene *nir*B in nitrogen metabolism was up-regulated under the high sodium nitrite concentration for enhancing denitrification (Zeng et al., 2018). However, the intracellular label of *nir*B and the response to nitrite concentration to reveal the regulation mechanism need further research. Enhanced green fluorescent protein (EGFP) can be used as a reporter protein with cell organelle-specific targeting and retaining signals for clarifying protein intracellular localization and functional analyses (Okino et al., 2018). The fluorescent protein can track the labeled bacteria cells survival under stress conditions, and aggregate in the cytosol when highly expressed in bacteria expression systems (Gao et al., 2020).

The study aims to investigate the potential mechanism of *L. fermentum* RC4 degrading nitrite in terms of genome, response and regulation. The whole genome analysis of *L. fermentum* RC4 was processed to identify pathways related to nitrite degradation. The EGFP labeled *L. fermentum*-EGFP-*nir*B was constructed to confirm the NirB expression activity under nitrite stress conditions. The overexpression strain *L. fermentum*-NirB was constructed to evaluate the nitrite degrading effect, and integrated with RNA-seq to find the metabolism pathways involved in nitrite degrading. The study will provide new insight into the construction of recombinant *L. fermentum* RC4 serving as a model strain to decrease nitrite in salted food.

2. Materials and methods

2.1. Materials

L. fermentum RC4 was preserved at the China General Microbiological Culture Collection Center (CGMCC NO. 8212). De Man, Rogosa and Sharpe (MRS) agar and broth medium were purchased from Qingdao Hope Bio-Technology Co., Ltd. (Shandong, China), and the Luria-Bertani (LB) medium was purchased from Fuyuan Biotch Co., Ltd. (Shanghai, China). The pET-28a-EGFP plasmid was purchased from Fenghui Biotech Co. Ltd (Hunan, China), and the Stbl3 *E. coli* competent cells were purchased from TransGen Biotech Co., Ltd. (Beijing, China). Polyethylene glycol (PEG) 20000 was purchased from Solarbio Technology Co., Ltd. (Beijing, China). The genomic DNA extraction kit, plasmid extraction kit, gel recycling kit, and reverse transcription PCR kit were obtained from Omega Bio-tek, Ink. (Georgia, USA). TemplatePrepKit 1.0 kit was obtained from KAPA Biosystems (Massachusetts, USA). ClonExpress II One Step Cloning Kit, and Ribo-off rRNA Depletion kit were obtained from Nanjing Vazyme Biotech Co., Ltd. (Jiangsu, China). HiPure Bacterial RNA Kit was obtained from Magen Biotech Co., Ltd. (Shanghai, China). The nitrite reductase activity assay kit was purchased from Suzhou Comin Biotech Co., Ltd. (Jiangsu, China). The nitrite detection kit was purchased from Nanjing Jiancheng Technology Co., Ltd. (Jiangsu, China). Other reagents are analytical grade.

2.2. Bacterial strains growth condition and whole genome sequencing

L. fermentum RC4 was incubated in MRS agar medium at 37 °C for 12–16 h. The single colony was selected and inoculated into MRS broth. The bacterial culture was grown to the logarithmic growth phase at 37 °C. A volume of 200 μL well-mixed bacterial suspension was dispensed into each of three replicate wells in a 96-well plate, and the optical density at 600 nm (OD_{600}) was measured to reach a value of 0.6–0.8 using the Infinite 200 pro plate reader (TECAN, Switzerland). Bacteria were collected by centrifugation (Centrifuge 5804 R, Eppendorf) at 7000 rpm for 5 min at 4 °C, and washed three times with phosphate-buffered saline and stored at −80 °C. Genomic DNA extraction kit was used to extract total DNA. TemplatePrepKit 1.0 kit was used to build the genomic library. The amplified library was sequenced using the Pacbio Sequel system. The data obtained by Pacbio Sequel were assembled using Unicycler and Flye software to obtain contig sequences, and then the contig results were corrected using Pilon software to assemble the complete sequence (Walker et al., 2014).

2.3. Construction of fluorescent-labeled recombinant expression *L. fermentum RC4*

2.3.1. Cloning of nirB and egfp

The sequence of *nir*B gene and pET-28a-EGFP plasmid was acquired from the National Center for Biotechnology Information (NCBI) (Bethesda, MD, USA). The primers of *nir*B and *egfp* gene were designed using Primer 5 and CE Design V1.04 (Table S1). The sites for restriction digestion are 5′ terminal *Sal I* and 3′ terminal *Hin*d III. The primers were synthesized by Sangon Biotech Co., Ltd. (Shanghai, China). The pET-28a-EGFP plasmid was transferred into Stbl3 *E. coli* competent cells by heat shock and the mixture was coated on Luria-Bertani (LB) medium with 50 μg/mL kanamycin. pET-28a-EGFP plasmid was extracted by a small volume plasmid extraction kit and stored at −20 °C. PCR was performed to amplify the *nir*B and *egfp* (Table S2). The PCR products were purified by agarose gel electrophoresis at 120 V for 30 min and recovered using the gel recycling kit.

2.3.2. Construction of recombinant plasmid pMG36e-EGFP-nirB

pMG36e was extracted by plasmid extraction kit from *E. coli*, and double digestion by *Sal* I and *Hind* III restriction endonuclease at 37 °C for 5 min (Table S3). The targeted genes of *nir*B and *egfp* and plasmid pMG36e were sequenced by Sangon Biotech. The construction of recombinant plasmid pMG36e-EGFP-*nir*B was performed by ClonExpress II One Step Cloning Kit (Table S4). The recombined products were transferred into *E. coli* competent cells by heat shock at 42 °C after being placed in an ice bath for 30 min. The recombinant cells were coated on LB agar medium with 100 μg/mL kanamycin to screen the positive clones identified by PCR and sequenced by Sangon Biotech.

2.3.3. Construction of recombinant L. fermentum-EGFP-nirB

Single colonies were selected and cultured overnight in MRS broth. A total volume of 2 mL inoculum was plated in MRS broth with 0.5% glucose and 0.5% glycine until OD_{600} of 0.6–0.8, and collected by centrifugation at 3000 rpm for 10 min. Sterile deionized water and A solution (10% glycerol and 10% sucrose, v/v) were precooled to 0 °C and wash bacteria twice. Centrifugation and resuspended bacteria in A solution. The bacteria are frozen in liquid nitrogen and stored at −80 °C. Gently mix 2 μL of pMG36e-EGFP-*nir*B and 100 μL of *L. fermentum* RC4 competent cells in sterile tubes, and electroporated at 1.2 kV for 4 ms. Add 1 mL pre-cooled MRS broth and resuscitate at 37 °C for 3 h. Fluorescent labeled and control strains were named *L. fermentum*-EGFP-*nir*B and *L. fermentum*-0, respectively. PCR was performed with primer pMG36e F/R for verification (Tables S5 and S6).

2.3.4. The expression activity of L. fermentum-EGFP-nirB at different concentrations of nitrates

0, 100, 200, 300, 400, and 500 mg/mL nitrate-contained MRS broth were prepared and incubated with 2% *L. fermentum* RC4 inoculum at 37 °C for 8 h. The fluorescent density was visualized by Nikon A1R confocal laser scanning microscope (CLSM) (Tokyo, Japan). The excitation light was selected as green, the excitation wavelength was 488 nm and the receiver wavelength was 550 nm.

2.4. Construction of overexpression L. fermentum-NirB

2.4.1. Cloning of nirB, construction of recombinant plasmid pMG36e-nirB and overexpression L. fermentum-NirB

The same steps were followed in section 2.2. PCR was performed to amplify *nir*B (Tables S7 and S8). The reaction system for the construction plasmid pMG36e-*nir*B is followed in Table S9. Electrotransformation was used to transform pMG36e-*nir*B into *L. fermentum* named *L. fermentum*-NirB and the control strain named *L. fermentum*-0. Plasmid pMG36e was resistant to erythromycin, detecting the maximum erythromycin tolerance concentration of *L. fermentum* RC4 to screen positive clones. *L. fermentum* RC4 was coated on 0, 1, 2, 3, 4, 5, 6, and 7 μg/mL erythromycin MRS plates at 37 °C for 48 h to detect the maximum erythromycin tolerance. The L. *fermentum*-NirB strains were coated on erythromycin MRS plates to screen the positive clones verified by PCR.

2.4.2. qPCR analysis of nirB expression

The total RNA was extracted according to the HiPure Bacterial RNA Kit. The reverse transcription PCR kit was used to obtain cDNA (Table S10). 16S rRNA was the internal reference for *nir*B. The 16S rRNA PCR primers were designed according to Kim et al. (Table S11) (Kim et al., 2014). The $2^{-\Delta\Delta Ct}$ method was used to calculate the expression of gene (Livak and Schmittgen, 2002). In order to minimize errors in the qPCR, the addition of cDNA was expanded to 5 μL, and other components in the reaction system were equally expanded (Table S12).

2.4.3. Determination of nitrite reductase content, NirB activity, growth curve and nitrite degradation rate

The extraction and purification of nitrite reductase were according to previous studies with some modifications. The recombinant L. *fermentum*-NirB and *L. fermentum*-0 were inoculated into MRS broth at 37 °C for 12–16 h. Lysozyme was added to the culture for cell wall disruption for 2 h, followed by ultrasonic treatment at 36 kHz for 15 min. The supernatant was collected by centrifugation at 12000 rpm for 15 min at 4 °C. The crude extract was precipitated using ammonium sulfate at 4 °C for 6 h and centrifugation at 5000 rpm for 30 min, followed by dialyzed against deionized water at room temperature for 5 d (Ferroni et al., 2012). The dialysis bag was embedded with PEG 20000 to concentrate the sample. The nitrite reductase content was determined by the method of ultraviolet absorption at 280 nm, with bovine serum albumin (BSA) as standard. NirB enzyme activity was determined by the nitrite reductase activity assay kit. The growth curve of recombinant strains was determined for 36 h at OD_{600}. The nitrite content was determined every 5 h by the nitrite detection kit.

2.5. RNA-seq analysis of L. fermentum-NirB

The total RNA was extracted followed by section 2.3.2. mRNA was purified by Ribo-off rRNA Depletion kit. The quality of extracted RNA using the Agilent Bioanalyzer 2100 Bioanalyzer (Agilent Technologies, Inc., USA). The cDNA libraries were sequenced using Illumina Hiseq 4000. Differentially expressed genes (DEGs) were screened based on log2 Fold Change > 1 and significance $p < 0.05$. Gene Ontology (GO) (https://geneontology.org) was performed to identify the biological function. The Kyoto Encyclopedia of Genes and Genomes (KEGG) Pathway (https://www.genome.jp/kegg/pathway.html) was performed to analyze the enrichment characteristics of the significant DEGs.

2.6. Data analysis

All the experiments were repeated three times. SPSS 22.0 (IBM, USA) was used to analyze statistics. Experimental differences were determined using one-way ANOVA and Duncan test at 0.05 levels. Graphpad Prism 9 and Adobe Illustrator 2022 were utilized for generating the figures. The CGView was used to draw the circular genome map (Stothard et al., 2017). The ggplot2 was employed for generating volcano plots, the Pheatmap was utilized for cluster analysis, and the topGO was used for screen enrichment GO terms.

3. Results

3.1. Genome sequence analysis of L. fermentum RC4

The gene features of *L. fermentum* RC4 might provide the basis for the nitrite degradation mechanism. The sequence length of *L. fermentum* RC4 was 2,060,268 bp, with GC content of 51.20% (Fig. 1). The genome sequence of *L. fermentum* RC4 was submitted to NCBI with accession number PRJNA976665. Carbohydrate-active enzyme database (CAZy) including glycoside hydrolases (GHs), glucosyl transferases (GTs), polysaccharide lyases (PLs), carbohydrate esterases (CEs), auxiliary activities (AAs) and carbohydrate-binding modules (CMBs). The higher gene number of GTs and GHs showed *L. fermentum* RC4 has the potential to resist pathogens and immune stimulation (Fig. S1 and Appendix B.) (Liu et al., 2022). Evolutionary genealogy of genes Non-supervised Orthologous Groups (eggNOG) annotation suggested that the dominance genes are related to amino acid, nucleotide, carbohydrate and coenzyme transport and metabolism (Fig. S2). These key genes within the carbohydrate and amino acid pathways may be involved in the energy metabolism and stress tolerance of *L. fermentum* RC4 to regulate the nitrite degradation process.

3.2. Construction of L. fermentum-EGFP-nirB and the effect of nitrate concentrations on NirB activity

3.2.1. Construction of fluorescent-labeled recombinant expression plasmid pMG36e-EGFP-nirB

L. fermentum RC4 grew on erythromycin plates at a concentration of 0–4 μg/mL and ceased to grow as the concentrations increased from 5 to 7 μg/mL (Fig. S3). Choose 5 μg/mL erythromycin as culture concentrations for recombinant *L. fermentum* RC4. The agarose gel electrophoresis amplified band of the purification *egfp* and *nir*B genes were clear and bright (Fig. 2 A and Fig. 2 B). The two bands were between 600-800 bp and 1000–1500 bp, respectively, which were consistent with the target gene (717 bp for *egfp* and 1350 bp for *nir*B). The primers were high specificity and the PCR amplification conditions were suitable for efficient amplification of the targeted fragments. The PCR products were 100% similar to the *egfp* and *nir*B sequences, indicating that the targeted fragments were correct for PCR. The vector plasmid pMG36e was double digestion by *Sal* I and *Hind* III restriction, with a 14 bp interval between digestion sites. The DNA marker indicated a minimum length of 100 bp for agarose gel electrophoresis. There was a single lane appeared in the electrophoresis (Fig. 2 C). The sequence results were compared to the pMG36e sequence, and selected successful digestion plasmid. The recombinant plasmid pMG36e-EGFP-*nir*B was constructed (Fig. S4). The PCR amplification of recombinant *L. fermentum* RC4 bands is uniform without trailing traces (Fig. 2 D). The length of the bands was 3444 bp which means the recombinant plasmid was successfully transferred into *L. fermentum* RC4. DNAMAN results showed that the sequence was completely overlapping with the target sequence, indicating recombinant plasmid has been constructed.

3.2.2. The expression activity of NirB at different nitrate concentrations

The recombinant plasmid pMG36e-EGFP-*nir*B was electrotransformed to *L. fermentum* RC4 resulting in the linkage of *egfp* and *nir*B.

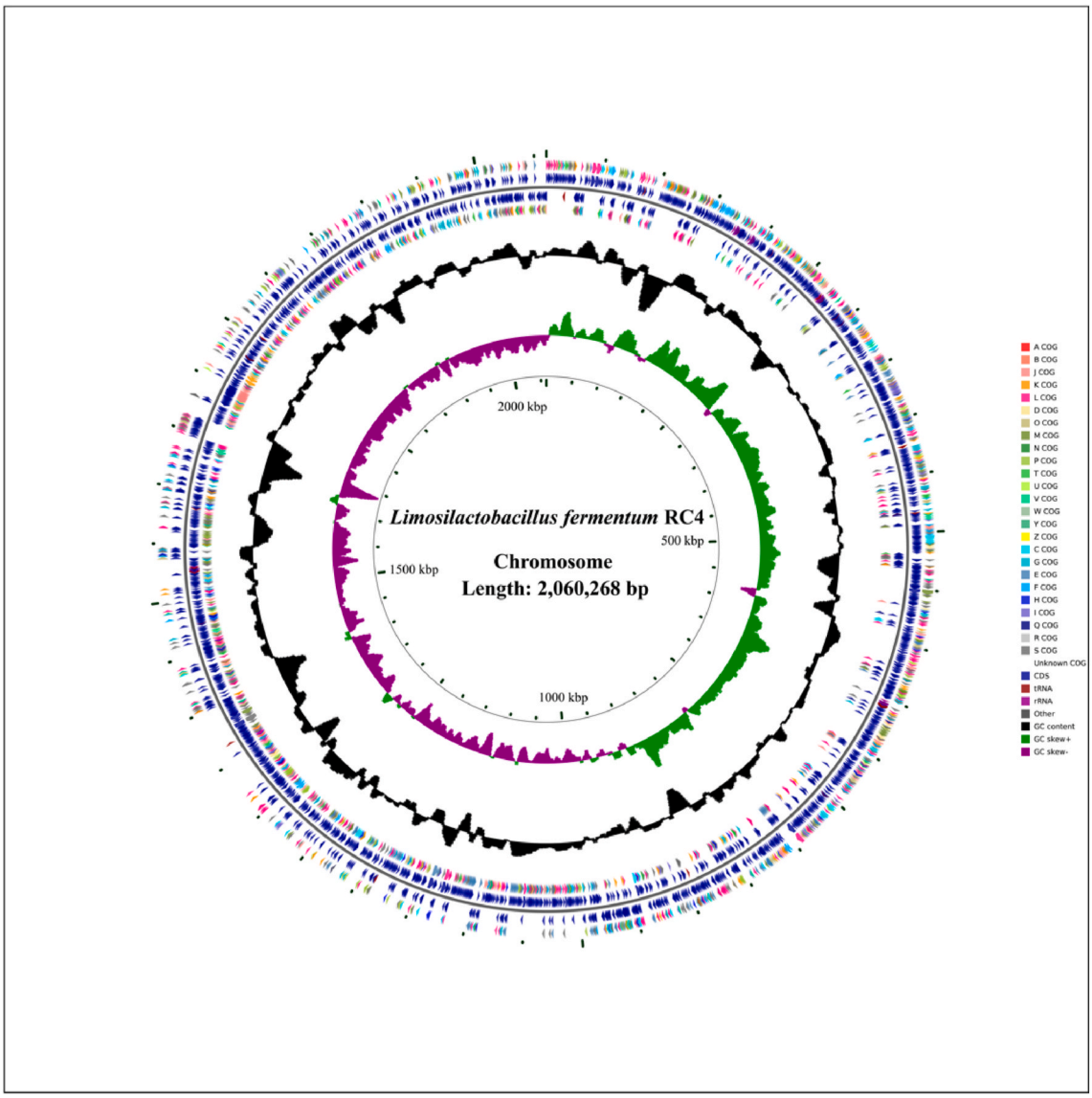

Fig. 1. The genome map of *L. fermentum* RC4. The first circle represents the scale. The second circle represents GC skew, which is used to measure the difference in the relative content of bases G and C in single-stranded DNA. The calculation method is (nG - nC)/(nG + nC), the content of G is greater than C is recorded as GC skew+, and the content of G is less than C is recorded as GC skew-. The third circle represents the GC content. The fourth and seventh circles represent each coding sequence CDS (Coding sequence) belonging to COGs (Cluster of orthologous groups). The fifth and sixth circles represent the positions of CDS, tRNA and rRNA on the genome.

It was observed that the NirB produced by *L. fermentum*-EGFP emitted intense green fluorescence under the excitation wavelength of 488 nm, whereas the blank control group exhibited a weaker response (Fig. 2 E). The intensity of NirB expression activity can be assessed based on the density of the observed green fluorescence. Each green fluorescent spot represents nitrate reductase NirB, and all recombinant *L. fermentum* RC4 is normally active when observed by CLSM. The green fluorescence density increased with the nitrate concentrations enhanced, reaching a maximum at concentrations of 300 mg/L and then began to decrease. NirB has higher enzyme activity under 300 mg/L nitrite.

3.3. The effect of NirB on L. fermentum RC4 growth and nitrite degradation

3.3.1. Construction of recombinant plasmid pMG36e-nirB

The recombinant plasmid pMG36e-*nir*B was constructed (Fig. S5). The PCR amplification of recombinant *L. fermentum* RC4 bands was single and bright without trailing (Fig. 3 A and Fig. 3 B). The length of the pMG36e plasmid band is 1377 bp, and the length of the recombinant pMG36e-*nir*B band is 2727 bp. It indicates that the recombinant plasmid was successfully transferred into *L. fermentum* RC4. The DNAMAN comparison results showed that the PCR products overlapped with the target sequences, indicating that the recombinant plasmid was successfully constructed.

3.3.2. qPCR analysis, nitrite reductase content, NirB enzyme activity, growth curve and nitrite degradation rate of recombinant L. fermentum-NirB

The qPCR results indicated that the expression level of the *nir*B gene in the recombinant strain *L. fermentum*-NirB was 3.17 times higher than that in the control strain *L. fermentum*-0 ($p < 0.0001$), suggesting that *nir*B gene was successfully overexpressed in *L. fermentum* RC4 (Fig. 3 C). The nitrite reductase content of *L. fermentum*-NirB was 217.39 mg/mL, 19.7% higher than *L. fermentum*-0 (Fig. 3 D). The NirB enzyme activity of *L. fermentum*-NirB is 381.8 U/L which increased 39.6% compared to the control group (273.5 U/L) (Fig. 3 E). The logarithmic period of the recombinant strains was 3–10 h, and the growth rate gradually decreased

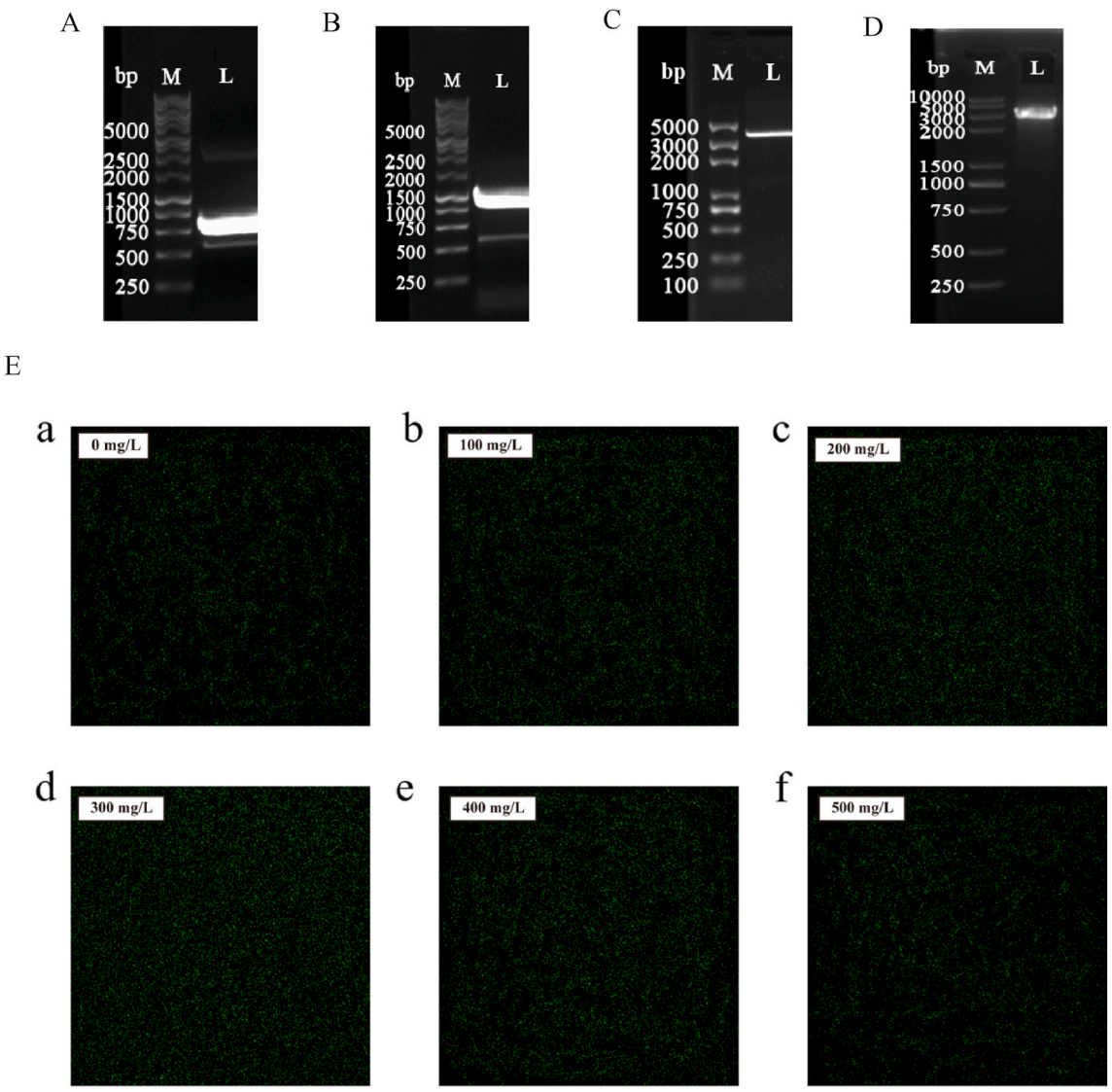

Fig. 2. The construction of fluorescence labeling strain *L. fermentum* -EGFP. (A) Electrophoresis of PCR amplified gene. M: DNA Marker. L: PCR product of *egfp* gene. (B) Electrophoresis of PCR amplified gene. M: DNA Marker. L: PCR product of *nir*B gene. (C) Electrophoresis of pMG36e plasmid digestion. M: DNA Marker. L: Plasmid digestion product of pMG36e. (D) PCR verification of pMG36e-EGFP-*nir*B recombinant plasmid. M: DNA Marker. L: PCR product of pMG36e-EGFP-*nir*B. (E) Green fluorescence of recombinant strain *L. fermentum*-EGFP under different nitrite concentrations. a–f: the nitrite concentration of 0 mg/L, 100 mg/L, 200 mg/L, 300 mg/L, 400 mg/L, and 500 mg/L. (For interpretation of the references to color in this figure legend, the reader is referred to the Web version of this article.)

after 10 h and entered the stable period. The growth rate and OD_{600} values of *L. fermentum*-0 were smaller than *L. fermentum*-NirB (Fig. 3 G). The nitrite degradation rates for the overexpression group and the control group under 300 mg/L nitrite were 9% and 8% within the first 5 h, respectively. The nitrite degradation rate was significantly accelerated after 5 h, which reached *L. fermentum*-NirB of 29% and *L. fermentum*-0 of 24.7%. Up to 40 h, the nitrite concentration of the overexpression strain was 25 mg/L with the degradation rate of 91.7%, and the control group was 51 mg/L and 83%, increased 10.5% compared to the control group (Fig. 3 F).

3.4. RNA-seq analysis of the effect and regulatory mechanism of NirB on the degradation of nitrite by L. fermentum RC4

3.4.1. DEGs screening and analysis

Transcriptomics could provide large findings about DEGs, novel genes, and detecting transcriptome expression of LAB (Li et al., 2022). *L. fermentum*-0 and *L. fermentum*-NirB were represented as L0 and L1. The percentage of bases recognition rates above 99% (Q20) reached 97.92% and 97.69%, and the percentage of bases recognition rates above 99.9% (Q30) reached 94.39% and 93.80%, respectively. The reference genome index was created by Bowtie2 (http://bowtie-bio.sourceforge.net/index.shtml), and compared the filtered Reads to the reference genome. The compliance rate of L0 and L1 groups reached 96.77% and 94.33%, respectively, and there was no significant difference between the three parallels in each group ($p > 0.05$). The results of library and RNA sequencing could accurately reflect the actual situation of the samples. A total of 474 gene expressions were significantly changed in L1 compared to L0, including 240 genes up-regulated and 234 genes down-regulated, accounting for 50.6% and 49.4% of the total DEGs, respectively (Fig. 4 A and Appendix C.). The biological information of the three parallel groups of L0 and L1 was of good quality, and the overexpression of NirB enzyme resulted in significant changes in the recombinant *L. fermentum* RC4 at the transcriptome level (Fig. 4 B).

3.4.2. GO and KEGG pathway analysis

GO enrichment analysis can provide an in-depth understanding of the functional distribution of DEGs. TopGO has three ontological

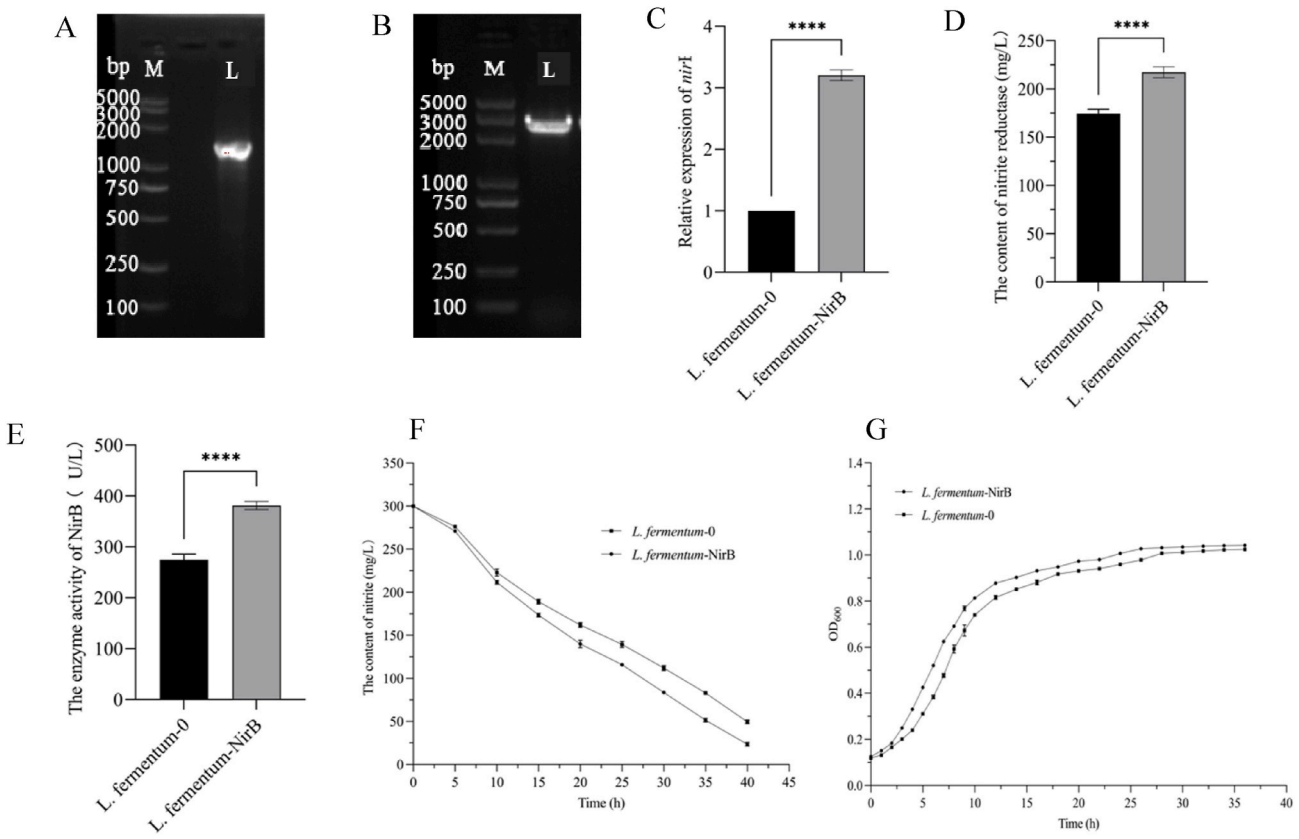

Fig. 3. The overexpression of NirB in *L. fermentum* RC4. (A) PCR verification of plasmid pMG36e. M: DNA Marker. L: PCR product of pMG36e. (B) PCR verification of plasmid pMG36e-nirB. M: DNA Marker. L: PCR product of pMG36e-nirB. (C) Relative expression of *nir*B in overexpression strains. (D) The content of nitrite reductase in recombinant *L. fermentum* RC4. (E) The enzyme activity of recombinant *L. fermentum* RC4. (F) The nitrite degradation curve of recombinant *L. fermentum* RC4. (G) The growth curve of recombinant *L.fermentum* RC4 at 300 mg/mL nitrite concentration. Asterisk (****) means $p < 0.0001$.

classification annotations: biological process (BP), cellular component (CC), and molecular function (MF). A total of 894 DEGs in *L. fermentum*-0 and *L. fermentum*-NirB were classified into three functional categories in GO, with 456 genes enriched in BP, 347 genes enriched in CC, and 91 genes exhibiting differences in MF (Fig. 4 C and Appendix D.). Regarding BP, notable changes were observed in pathways such as the organonitrogen compound biosynthetic and metabolic process, organic acid biosynthetic process, and amino acid biosynthetic and metabolic process. In terms of CC, significant differences were observed in genes related to ribosome, ribonucleoprotein complex, organelle, non-membrane-bound organelle, cytoplasmic ribosome, and protein-containing complex. For MF, the DEGs were primarily enriched in the structural constituent of ribosome, structural molecule activity, binding, cofactor binding, oxidoreductase activity, RNA binding and other regions.

The changes in major metabolic pathways were revealed by KEGG Pathway enrichment analysis (Fig. 4 D). A total of 346 DEGs were annotated and involved in 85 metabolic pathways, with 248 DEGs (71.68%) categorized into metabolic pathways, and 54 DEGs (15.61%) classified as related to genetic information processing. Additionally, a total of 24, 16, and 4 DEGs were associated with environmental information processing, human diseases, and cellular processes, respectively. The main changed metabolic pathways include carbohydrate metabolism, amino acid metabolism and energy metabolism.

3.4.3. Carbohydrate metabolism and amino acid metabolism gene analysis

The overexpression of *nir*B stimulates genetic changes related to the carbohydrate and amino acid metabolic pathways according to the KEGG results. The representative DEGs were distributed in a variety of carbohydrate and amino acid metabolic pathways (Table 1). The DEGs in carbohydrate metabolism mainly focus on pyruvate metabolism, glycolysis/gluconeogenesis, citrate cycle (TCA cycle), starch and sucrose metabolism, amino and nucleotide sugar metabolism, and pentose phosphate pathway. A total of 69 genes were involved in the carbohydrate metabolism pathway, containing 43 up-regulated genes and 26 down-regulated genes. The DEGs in amino acid metabolism mainly focused on cysteine and methionine metabolism, arginine biosynthesis et al. There are 31 up-regulated genes and 28 down-regulated genes in the amino acid metabolic.

4. Discussion

L. fermentum RC4 can be effectively used in the control nitrite content in fermented foods, however more sufficient evidence of the mechanism during the process especially enzyme expression level and *nir*B intracellular label is needed. The whole genome sequence results reveal that *L. fermentum* RC4 has the potential of adaptability and stress resistance to environment, which provides a base for the following research. *L. fermentum*-EGFP-*nir*B as the model strain, the main features of fluorescence labeling NirB was investigated. The plasmid fragment connected *egfp-nir*B can respond to a specific nitrite environment, and reporter protein EGFP will be expressed. The fluorescence intensity of the reporter protein can be used as an indicator to reflect the concentration of the nitrite. In order to clarify the regulatory role of *nir*B in denitrification and nitrogen metabolism, the *L. fermentum*-NirB was constructed with the plasmid pMG36e-*nir*B, which shows a better nitrite degrading effect.

EGFP exhibits photostability under low light conditions and generates a single absorption band peaking near 490 nm resulting in the phenolate anion of Tyr66 (Herman et al., 2018). The fluorescence

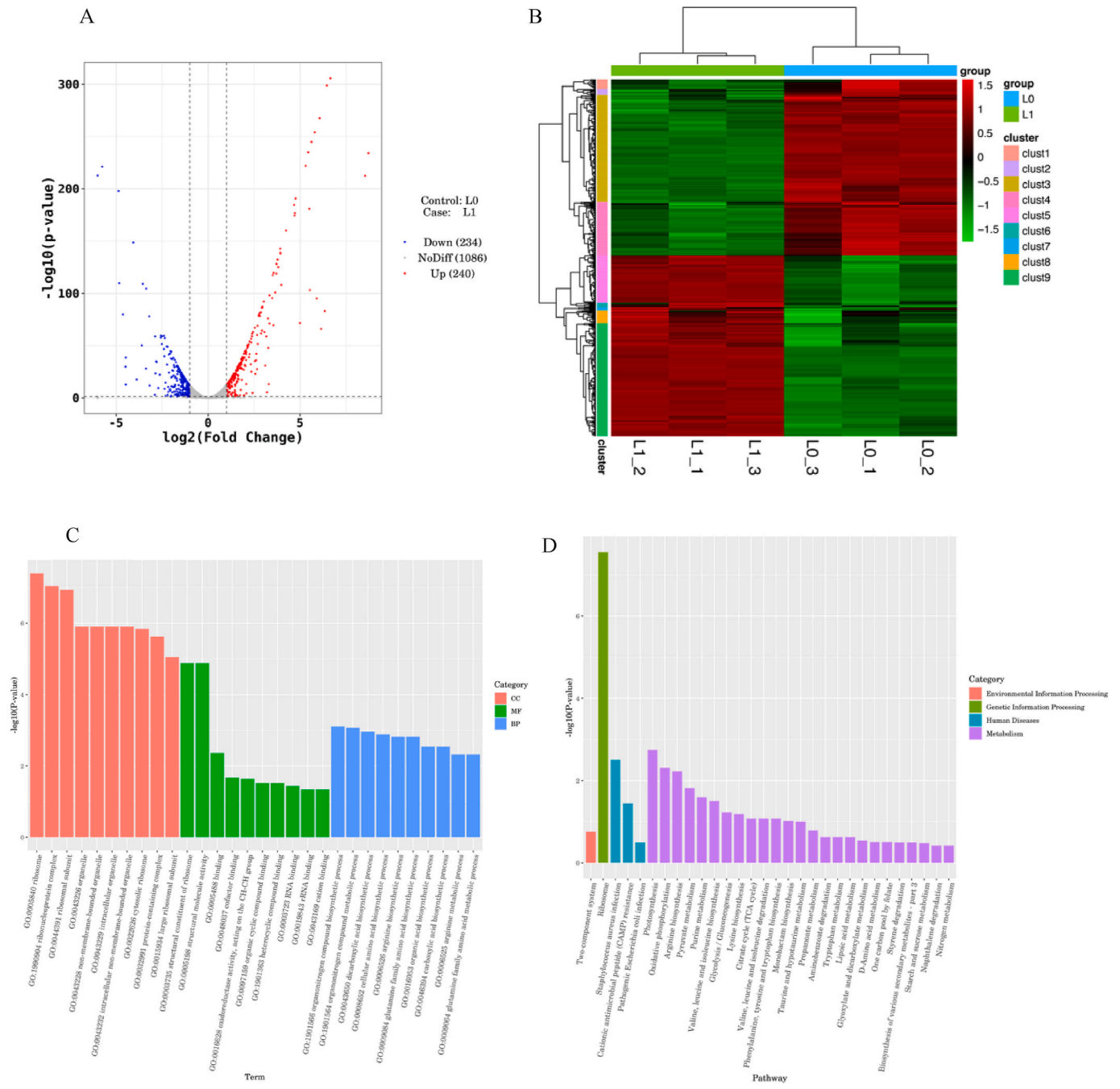

Fig. 4. RNA-seq of NirB on the degradation of nitrite by *L. fermentum* RC4. Recombinant strains L. *fermentum*-0 and *L. fermentum*-NirB are represented as L0 and L1. (A) The volcano plot of DEGs. The x-coordinate is log2FoldChange and the y-coordinate is -log10 (p-value). The two vertical dotted lines in the figure represent the threshold of twice the expression difference. The horizontal dotted line indicates the threshold of P-value = 0.05. Red dots indicate up-regulated genes, blue dots indicate down-regulated genes, and gray dots indicate non-significant DEGs. (B) The clustering of DEGs. Horizontally representing genes, each column presents one sample. Red indicates high-expression genes and green indicates low-expression genes. (C) GO analysis of DEGs. The x-coordinate is the term of Go level2, and the y-coordinate is -log10 (p-value) enriched in each term. (D) KEGG pathway enrichment of DEGs. The x-coordinate is pathway name, and the y-coordinate is -log10 (p-value) enriched in each pathway. (For interpretation of the references to color in this figure legend, the reader is referred to the Web version of this article.)

intensity detected by EGFP in each cell was higher, and the proportion of cells below the fluorescence detection threshold was lower, which facilitated the observation by microscopy (Garay-Novillo et al., 2019). The L. *fermentum*-EGFP could monitor NirB within the concentration of 0–500 mg/L nitrite via the fluorescence intensity of expressed EGFP. The fluorescence performance at 0–300 mg/L nitrite concentration can be speculated that nitrite concentration in the environment is positively correlated with NirB expression activity (Song et al., 2020). The pH values of the recombinant *L. fermentum*-EGFP culture media were greater than 4.0, indicating that the enzymatic degradation was the primary mechanism for nitrite degradation (Huang et al., 2021). NirB is a nitrogen cycle ammonification pathway enzyme that catalyzes the conversion of NO_2^- to NH_4^+ and can decrease nitrite in the cytoplasm under anaerobic conditions with NADH as an electron donor (Yılmaz et al., 2022). The NirC protein is responsible for this transport. The density of green fluorescence diminishes when the nitrite concentration is 400 and 500 mg/ml, and this could be because the high nitrite concentrations impeded the growth of *L. fermentum* RC4. The OD_{600} of 400

Table 1
Genes related to carbohydrate metabolism and amino acid metabolism.

	Gene	Encoded protein	Expression trend
Carbohydrate metabolism	*ldh*A	D-lactate dehydrogenase	↑
	ldh	L-lactate dehydrogenase	↑
	*ace*E	Pyruvate dehydrogenase E1 component	↑
	*ack*A	Acetic kinase	↑
	*pdh*D	Dihydrolipoamide dehydrogenase	↑
	*ace*F	Pyruvate dehydrogenase E2	↑
	pta	Phosphate acetyltransferase	↑
	*adh*E	Acetaldehyde dehydrogenase/ ethanol dehydrogenase	↑
	*gal*M	Aldose 1-epimerase	↑
	*gap*A	Glyceraldehyde 3-phosphate dehydrogenase	↑
	pgk	Phosphoglycerate kinase	↑
	*gpm*A	Phosphoglyceride mutase	↑
	*gal*U	Utp-glucose-1-phosphouridine transferase	↑
	*sfc*A	Malate dehydrogenase	↓
	*adh*P	Alcohol dehydrogenase	↓
	ACACA	Acetyl-CoA carboxylase/biotin carboxylase	↓
	SPP	Sucrose 6-phosphatase	↓
	*sac*A	β-furanosidase	↓
	*scr*K	Fructokinase	↓
	pgi	Glucose-6-phosphate isomerase	↓
Amino acid metabolism	*ser*A	D-3-phosphoglycerate dehydrogenase	↑
	ldh	L-lactate dehydrogenase	↑
	*ilv*E	Amino acid transaminase	↑
	*mtn*N	Cysteine ribosidase	↑
	*met*K	Methionine synthetase	↑
	*gpm*A	Phosphoglyceride mutase	↑
	*gar*K	Glycero-2-kinase	↑
	*pdh*D	Dihydrolipoamide dehydrogenase	↑
	*aro*K	Shikimate kinase	↑
	*aro*C	Chordal synthase	↑
	*tyr*A2	Prebenzoic acid dehydrogenase	↑
	*dap*E	Acrylamide desuccinase	↓
	*dap*B	4-hydroxytetrahydropyridine reductase	↓
	*dap*A	4-hydroxytetrahydrodipyridinate synthase	↓
	*lys*A	Sodium diaminoacrylate decarboxylase	↓

and 500 mg/L nitrite medium is significantly lower than the other groups. It indicates that excessive nitrite concentration might inhibit the growth of *L. fermentum* RC4, which results in decreased NirB enzyme expression activity. Besides, the overexpression of *nir*B gene could effectively increase the content of nitrite reductase by 42.83 mg per unit. Nitrite degradation relies on pH conditions. The final pH of the culture media for the *L. fermentum*-NirB and *L. fermentum*-0 were 4.33 and 4.53, respectively, indicating that enzymatic degradation is dominant. According to the growth curve, the recombinant *L. fermentum*-NirB entered the logarithmic growth phase after 5 h, during which the bacterial metabolism was robust and acid production increased. In the previous study, the substances produced by *L. fermentum* RC4 exhibited effective nitrite degradation ability, particularly when synergistically combined with acids (Xia et al., 2022). Representative metabolites, such as trans-aconitic acid, MTP, isocitric acid, and lysine, are capable of degrading nitrite through mechanisms including decarboxylation reactions, providing energy, and promoting enzymatic activity. It can be speculated from the trend that NirB enzyme overexpression indicates a significant promotion of nitrite degradation.

The representative DEGs expression in the carbohydrate and amino acid metabolism were investigated by RNA-seq. *L. fermentum* RC4 is a facultative anaerobe bacteria that obtains ATP energy derived from glycolysis, pyruvate and amino acid metabolism. Genes involved in gluconeogenesis and glycolysis, the *ldh* gene for lactate dehydrogenase (LDH), *gap*A gene for glyceraldehyde-3-phosphate dehydrogenase (GAPDH), *pgk* gene for phosphoglycerate kinase, *ace*E gene for pyruvate dehydrogenase E1 component, *adh*E gene for acetaldehyde dehydrogenase/alcohol dehydrogenase, and *gal*M gene for aldose 1-epimerase, were up-regulated. LDH is a class of NAD-dependent kinases that catalyze the reduction and oxidation reactions between propionic acid and L-lactic acid, as well as the related α-keto acid (Jung et al., 2019). The decrease in LHD activity is one of the primary causes of bacterial damage after freeze drying (Kawai and Suzuki, 2007). GAPDH is a cytoplasmic protein involved in glycolysis and has crucial physiological functions (Deng et al., 2020). It is crucial for ensuring cell life because the activity level directly affects the survival rate of bacterial cells (Corcoran et al., 2005). The up-regulation of phosphoglycerate kinase (*pgk*), a crucial enzyme in glycolysis, accelerates the catalysis of the 1,3-bisphosphoglycerate to 3-phosphoglycerate, which serves as a precursor of lipoteichoic acid and mediate the characteristics of S-layer protein (Cai et al., 2020). Glycogenesis and glycolysis are the main pathways for energy acquisition in bacteria cells, during which glucose is catalyzed to produce pyruvate and energy, and pyruvate can be further reduced to lactate (Wu et al., 2016). It can be speculated that the enhanced cellular ATP and pyruvate synthesis supports higher survival rates of bacteria. In the same way, the up-regulation of genes that code for pyruvate metabolism-related enzymes, such as pyruvate dehydrogenase and phosphate acetyltransferase, speed up bacteria breakdown of pyruvate to make lactate and provide energy for cells. Besides, the up-regulation of acetate kinase (*ack*A) promotes pyruvate to acetate metabolism (Tojo et al., 2010), which is may available for LAB growth conditions to create acid to speed up the rate of nitrite breakdown.

Amino acid metabolism can assist the strain to resist changes in the external situation through metabolic regulation in a stressed environment (Le et al., 2022). Cysteine nucleotidases and methionine synthase were encoded by *mtn*N and *met*K, which are important enzymes for cysteine metabolism (André et al., 2008). In the overexpression group, the gene expression related to cysteine synthesis of *ser*A, *mtn*N and *ilv*E was up-regulated. Cysteine functions as an osmoprotectant to prevent cellular damage from hyperosmotic environments (Liu et al., 2015). In addition, cysteine is the immediate precursor for the synthesis of glutathione (GSH), which is a low molecular weight mercaptan compound and has antioxidant and scavenge intracellular free radicals properties (McBean, 2017). These up-regulated genes may help cells adapt to environmental stress through increases in the production of cysteine, which may be an important mechanism for decreasing nitrite. On the contrary, the down-regulation of arginase reduces the consumption of glutamic acid, which is the initial substrate for arginine biosynthesis (Huang et al., 2023). Glutamic acid and arginine are accumulated to help cells produce more energy and ammonia. The gene that codes for glutamine synthetase (*gln*A) is activated to help with the conversion of ammonia to pentamethylene diamine. Pentamethylene is a naturally occurring polyamine that can shield cells from H^+ toxicity in an acidic environment to sustain cell viability in the absence of phosphate and oxygen (Moreau, 2007). Interestingly, the expression of arginine deiminase encoding gene *arc*A was up-regulated, which facilitated the conversion of arginine to citric acid in the TCA cycle. The cycle was sped up and also benefited from the enhancement of acetyl-CoA by acetaldehyde dehydrogenase and ethanol dehydrogenase encoded genes *adh*E and *adh*P up-regulation. The down-regulation of malate dehydrogenase encoded gene *sfc*A inhibited the transformation of malic acid into oxaloacetic acid in the TCA. This enables the cells to quicken other metabolic pathways in order to collect the resources and energy required for survival functions (Takahashi-Íñiguez et al., 2018). It can be further speculated that expression levels of some key genes altered by up-regulated glycolysis, pyruvate and amino acid metabolism encoded genes to accumulate critical enzymes, indicating that the modulation of carbohydrate and amino acid metabolism system is one of the critical mechanisms to enhance the *L. fermentum* RC4 tolerance.

5. Conclusion

In summary, *L. fermentum* RC4 has the potential for stress tolerance related to key genes within the metabolism pathways. The fluorescent-labeled strain *L. fermentum*-EGFP-*nir*B strain was constructed for the first time, indicating NirB has a threshold as nitrite increases and reached its highest at 300 mg/L. NirB overexpressed in *L. fermentum* RC4 significantly enhanced the nitrite degradation rate, enzyme activity and nitrite reductase content. The RNA-seq showed that NirB significantly altered 248 differential genes mainly enriched in carbohydrate, amino acid metabolism, and energy metabolism. Interestingly, *ldh*, *gap*A and *pgk* for glycolysis/gluconeogenesis pathway, *ack*A for pyruvate metabolism, *ser*A, *mtn*N and *ilv*E for cysteine biosynthesis were significantly up-regulated. NirB regulates the physiological activities of bacteria to produce acid and respond to external environmental stress to enhance nitrite degradation rate. This study provides a guide for the use of NirB overexpressed in *L. fermentum* RC4 serving as a model strain to degrade nitrite during preserved food production.

CRediT authorship contribution statement

Qing Fan: Conceptualization, Investigation, Writing – original draft, Visualization. **Chaoran Xia:** Conceptualization, Investigation, Writing – original draft, Visualization. **Xiaoqun Zeng:** Supervision, Writing – review & editing, Project administration, Funding acquisition. **Zhen Wu:** Writing – review & editing, Validation. **Yuxing Guo:** Writing – review & editing, Validation. **Qiwei Du:** Writing – review & editing. **Maolin Tu:** Writing – review & editing. **Xinanbei Liu:** Writing – review & editing. **Daodong Pan:** reviewing, Validation, Funding acquisition.

Declaration of competing interest

The authors declare that they have no conflict of interest.

Data availability

No data was used for the research described in the article.

Acknowledgments

We gratefully acknowledge the financial support of the National Natural Science Foundation of China (32072195, 41406165, 41641052, 31972093, 31972048), the National Key Research and Development Program of China (2022YFD2100603), the Natural Science Foundation of Zhejiang Province for Diatinguished Young Scholars (LR23C200001).

Appendix A. Supplementary data

Supplementary data to this article can be found online at https://doi.org/10.1016/j.crfs.2024.100749.

References

André, G., Even, S., Putzer, H., Burguière, P., Croux, C., Danchin, A., et al., 2008. S-box and T-box riboswitches and antisense RNA control a sulfur metabolic operon of *Clostridium acetobutylicum*. Nucleic Acids Res. 36 (18), 5955–5969. https://doi.org/10.1093/nar/gkn601.

Cai, G., Wu, D., Li, X., Lu, J., 2020. Levan from *Bacillus amyloliquefaciens* JN4 acts as a prebiotic for enhancing the intestinal adhesion capacity of *Lactobacillus reuteri* JN101. Int. J. Biol. Macromol. 146, 482–487. https://doi.org/10.1016/j.ijbiomac.2019.12.212.

Chetty, A.A., Prasad, S., Pinho, O.C., de Morais, C.M., 2018. Estimated dietary intake of nitrate and nitrite from meat consumed in Fiji. Food Chem. 278, 630–635. https://doi.org/10.1016/j.foodchem.2018.11.081.

Corcoran, B.M., Stanton, C., Fitzgerald, G.F., Ross, R.P., 2005. Survival of probiotic lactobacilli in acidic environments is enhanced in the presence of metabolizable sugars. Appl. Environ. Microbiol. 71 (6), 3060–3067. https://doi.org/10.1128/aem.71.6.3060-3067.2005.

Deng, Z., Dai, T., Zhang, W., Zhu, J., Luo, X., Fu, D., et al., 2020. Glyceraldehyde-3-hosphate dehydrogenase increases the adhesion of *Lactobacillus reuteri* to host mucin to enhance probiotic effects. Int. J. Mol. Sci. 21 (24) https://doi.org/10.3390/ijms21249756. Article 9756.

dos Santos, B.A., da Fontoura, A.M., Correa, L.P., Pinton, M.B., Padilha, M., Fracari, P.R., et al., 2023. Jabuticaba peel extract and nisin: a promising combination for reducing sodium nitrite in Bologna-type sausages. Meat Sci. 204, 109273 https://doi.org/10.1016/j.meatsci.2023.109273.

Du, R., Song, G., Zhao, D., Sun, J., Ping, W., Ge, J., 2018. *Lactobacillus casei* starter culture improves vitamin content, increases acidity and decreases nitrite concentration during sauerkraut fermentation. Int. J. Food Sci. Technol. 53 (8), 1925–1931. https://doi.org/10.1111/ijfs.13779.

Duan, Y., Zhang, J., Wang, Y., Liu, Q., Xiong, D., 2018. Nitrite stress disrupts the structural integrity and induces oxidative stress response in the intestines of Pacific white shrimp *Litopenaeus vannamei*. J. Exp. Zool. Part A 329, 43–50. https://doi.org/10.1002/jez.2162.

Elias, A., Jalakas, S., Roasto, M., Reinik, M., Nurk, E., Kaart, T., et al., 2020. Nitrite and nitrate content in meat products and estimated nitrite intake by the Estonian children. Food Addit. Contam. 37 (8), 1129–1237. https://doi.org/10.1080/19440049.2020.1757164.

Fang, F., Feng, T., Du, G., Chen, J., 2016. Evaluation of the impact on food safety of a *Lactobacillus coryniformis* strain from pickled vegetables with degradation activity against nitrite and other undesirable compounds. Food Addit. Contam. 33 (4), 623–630. https://doi.org/10.1080/19440049.2016.1156774.

Ferroni, F.M., Guerrero, S.A., Rizzi, A.C., Brondino, C.D., 2012. Overexpression, purification, and biochemical and spectroscopic characterization of copper-containing nitrite reductase from *Sinorhizobium meliloti* 2011. Study of the interaction of the catalytic copper center with nitrite and NO. J. Inorg. Biochem. 114, 8–14. https://doi.org/10.1016/j.jinorgbio.2012.04.016.

Gao, H., Li, C., Ramesh, B., Hu, N., 2017. Cloning, purification and characterization of novel Cu-containing nitrite reductase from the *Bacillus firmus* GY-49. World J. Microbiol. Biotechnol. 34 https://doi.org/10.1007/s11274-017-2383-6. Article 10.

Gao, J., Qian, H., Guo, X., Mi, Y., Guo, J., Zhao, J., et al., 2020. The signal peptide of Cry1Ia can improve the expression of eGFP or mCherry in *Escherichia coli* and *Bacillus thuringiensis* and enhance the host's fluorescent intensity. Microb. Cell Factories 19. https://doi.org/10.1186/s12934-020-01371-8. Article 112.

Garay-Novillo, J.N., García-Morena, D., Ruiz-Masó, J.Á., Barra, J.L., Del Solar, G., 2019. Combining modules for versatile and optimal labeling of lactic acid bacteria: two pMV158-family promiscuous replicons, a pneumococcal system for constitutive or inducible gene expression, and two fluorescent proteins. Front. Microbiol. 10 https://doi.org/10.3389/fmicb.2019.01431. Article 1431.

Giguere, A.T., Taylor, A.E., Myrold, D.D., Mellbye, B.L., Sayavedra-Soto, L.A., Bottomley, P.J., 2018. Nitrite-oxidizing activity responds to nitrite accumulation in soil. FEMS (Fed. Eur. Microbiol. Soc.) Microbiol. Ecol. 3, 1–6. https://doi.org/10.1093/femsec/fiy008.

Herman, P., Holoubek, A., Brodska, B., 2018. Lifetime-based photoconversion of EGFP as a tool for FLIM. Biochim. Biophys. Acta Gen. Subj. 1863 (1), 266–277. https://doi.org/10.1016/j.bbagen.2018.10.016.

Hu, P., Ali, U., Aziz, T., Wang, L., Zhao, J., Nabi, G., et al., 2023. Investigating the effect on biogenic amines, nitrite, and N-nitrosamine degradation in cultured sausage ripening through inoculation of *Staphylococcus xylosus* and lactic acid bacteria [Original Research]. Front. Microbiol. 14 https://doi.org/10.3389/fmicb.2023.1156413.

Huang, L., Zeng, X., Sun, Z., Wu, A., He, J., Dang, Y., et al., 2019. Production of a safe cured meat with low residual nitrite using nitrite substitutes. Meat Sci. 162 https://doi.org/10.1016/j.meatsci.2019.108027. Article 108027.

Huang, S., Yang, X., Chen, G., Wang, X., 2023. Application of glutamic acid improved as tolerance in aromatic rice at early growth stage. Chemosphere 322. https://doi.org/10.1016/j.chemosphere.2023.138173. Article 138173.

Huang, Y.-y., Liu, D.-m., Jia, X.-z., Liang, M.-h., Lu, Y., Liu, J., 2021. Whole genome sequencing of *Lactobacillus plantarum* DMDL 9010 and its effect on growth phenotype under nitrite stress. LWT - Food Sci. Technol. (Lebensmittel-Wissenschaft -Technol.) 149, 111778. https://doi.org/10.1016/j.lwt.2021.111778.

Izumi, A., Schnell, R., Schneider, G., 2012. Crystal structure of NirD, the small subunit of the nitrite reductase NirbD from *Mycobacterium tuberculosis* at 2.0 Å resolution. Proteins: Struct., Funct., Bioinf. 80 (12), 2799–2803. https://doi.org/10.1002/prot.24177.

Jung, S., Hwang, H., Lee, J.-H., 2019. Effect of lactic acid bacteria on phenyllactic acid production in kimchi. Food Control 106, 106701. https://doi.org/10.1016/j.foodcont.2019.06.027.

Kawai, K., Suzuki, T., 2007. Stabilizing effect of four types of disaccharide on the enzymatic activity of freeze-dried lactate dehydrogenase: Step by step evaluation from freezing to storage. Pharmaceut. Res. 24, 1883–1890. https://doi.org/10.1007/s11095-007-9312-6.

Khlebodarova, T.M., Ree, N.A., Likhoshvai, V.A., 2016. On the control mechanisms of the nitrite level in *Escherichia coli* cells: the mathematical model. BMC Microbiol. 16, 15–30. https://doi.org/10.1186/s12866-015-0619-x.

Kim, S.-E., Choi, S.C., Park, K.S., Park, M.I., Shin, J.E., Lee, T.H., et al., 2014. Change of fecal flora and effectiveness of the short-term VSL#3 probiotic treatment in patients with functional constipation. Journal of Neurogastroenterology and Motility 21 (1), 111–120. https://doi.org/10.5056/jnm14048.

Le, Y., Lou, X., Yu, C., Guo, C., He, Y., Lu, Y., et al., 2022. Integrated metabolomics analysis of *Lactobacillus* in fermented milk with fish gelatin hydrolysate in different degrees of hydrolysis. Food Chem. 408, 135232 https://doi.org/10.1016/j.foodchem.2022.135232.

Li, Y., Xiong, D., Yuan, L., Fan, P., Xiao, Y., Chen, J., et al., 2022. Transcriptome and protein networks to elucidate the mechanism underlying nitrite degradation by

Lactiplantibacillus plantarum. Food Res. Int. 156 https://doi.org/10.1016/j.foodres.2022.111319. Article 111319.

Liu, D., Huang, Y., Liang, M., 2022. Analysis of the probiotic characteristics and adaptability of *Lactiplantibacillus plantarum* DMDL 9010 to gastrointestinal environment by complete genome sequencing and corresponding phenotypes. LWT - Food Sci. Technol. (Lebensmittel-Wissenschaft -Technol.) 158, 113129. https://doi.org/10.1016/j.lwt.2022.113129.

Liu, L., Si, L., Meng, X., Luo, L., 2015. Comparative transcriptomic analysis reveals novel genes and regulatory mechanisms of *Tetragenococcus halophilus in* response to salt stress. J. Ind. Microbiol. Biotechnol. 42 (4), 601–616. https://doi.org/10.1007/s10295-014-1579-0.

Livak, K.J., Schmittgen, T.D., 2002. Analysis of relative gene expression data using real-time quantitative PCR and the 2(-Delta Delta C(T)) Method. Methods 25 (4), 402–408. https://doi.org/10.1006/meth.2001.1262.

McBean, G.J., 2017. Cysteine, glutathione, and thiol redox balance in astrocytes. Antioxidants 6 (3). https://doi.org/10.3390/antiox6030062. Article 62.

Moreau, P.L., 2007. The lysine decarboxylase CadA protects *Escherichia coli* starved of phosphate against fermentation acids. J. Bacteriol. 189 (6), 49–61. https://doi.org/10.1128/jb.01306-06.

Okino, N., Wakisaka, H., Ishibashi, Y., Ito, M., 2018. Visualization of endoplasmic reticulum and mitochondria in *Aurantiochytrium limacinum* by the expression of EGFP with cell organelle-specific targeting/retaining signals. Mar. Biotechnol. 20, 182–192. https://doi.org/10.1007/s10126-018-9795-7.

Song, Q., Wang, B., Zhao, F., Han, Y., Zhou, Z., 2020. Expression, characterization and molecular docking of the assimilatory NaDH-nitrite reductase from *Acidovorax wautersii* QZ-4. Biochem. Eng. J. 105, 107589 https://doi.org/10.1016/j.bej.2020.107589.

Stepuro, I.I., Oparin, A.Y., Stsiapura, V.I., Maskevich, S.A., Titov, V.Y., 2012. Oxidation of thiamine on reaction with nitrogen dioxide generated by ferric myoglobin and hemoglobin in the presence of nitrite and hydrogen peroxide. Biochemistry (Moscow) 77, 41–55. https://doi.org/10.1134/s0006297912010051.

Stothard, P., Grant, J.R., Van Domselaar, G., 2017. Visualizing and comparing circular genomes using the CGView family of tools. Briefings Bioinf. 20 (4), 1576–1582. https://doi.org/10.1093/bib/bbx081.

Takahashi-Íñiguez, T., Barrios-Hernández, J., Rodríguez-Maldonado, M., Flores, M.E., 2018. Tricarboxylic acid cycle without malate dehydrogenase in *Streptomyces coelicolor* M-145. Arch. Microbiol. 200 (9), 1279–1286. https://doi.org/10.1007/s00203-018-1541-z.

Tiso, M., Schechter, A.N., 2015. Nitrate reduction to nitrite, nitric oxide and ammonia by gut bacteria under physiological conditions. PLoS One 10 (5). https://doi.org/10.1371/journal.pone.0119712. Article e0127490.

Tojo, S., Kumamoto, K., Hirooka, K., Fujita, Y., 2010. Heavy involvement of stringent transcription control depending on the adenine or guanine species of the transcription initiation site in glucose and pyruvate metabolism in *Bacillus subtilis*. J. Bacteriol. 192 (6), 1573–1585. https://doi.org/10.1128/jb.01394-09.

Walker, B.J., Abeel, T., Shea, T., Priest, M., Abouelliel, A., Sakthikumar, S., et al., 2014. Pilon: an integrated tool for comprehensive microbial variant detection and genome assembly improvement. PLoS One 9 (11). https://doi.org/10.1371/journal.pone.0112963. Article e112963.

Wu, Z., Wang, P., He, J., Pan, D., Zeng, X., Cao, J., 2016. Proteome analysis of *Lactobacillus plantarum* strain under cheese-like conditions. J. Proteonomics 146, 165–171. https://doi.org/10.1016/j.jprot.2016.07.008.

Xia, C., Tian, Q., Kong, L., Sun, X., Shi, J., Zeng, X., et al., 2022. Metabolomics analysis for nitrite degradation by the metabolites of *Limosilactobacillus fermentum* RC4. Foods 11 (7). https://doi.org/10.3390/foods11071009. Article 1009.

Yılmaz, H., İbici, H.N., Erdoğan, E.M., Türedi, Z., Ergenekon, P., Özkan, M., 2022. Nitrite is reduced by nitrite reductase NirB without small subunit NirD in *Escherichia coli*. J. Biosci. Bioeng. 134 (5), 393–398. https://doi.org/10.1016/j.jbiosc.2022.07.015.

Yu, S., Zhang, Y., 2013. Effects of Lactic Acid Bacteria on Nitrite Degradation during Pickle Fermentation, vols. 781–784, pp. 1656–1660. https://doi.org/10.4028/www.scientific.net/AMR.781-784.1656.

Zeng, X., Pan, Q., Guo, Y., Wu, Z., Sun, Y., Dang, Y., et al., 2018. Potential mechanism of nitrite degradation by *Lactobacillus fermentum* RC4 based on proteomic analysis. J. Proteonomics 194, 70–78. https://doi.org/10.1016/j.jprot.2018.12.021.

Zhu, Y., Wang, C., Jia, S., Wang, B., Zhou, K., Chen, S., et al., 2018. Purification, characterization and antioxidant activity of the exopolysaccharide from *Weissella cibaria* SJ14 isolated from Sichuan paocai. Int. J. Biol. Macromol. 115, 820–828. https://doi.org/10.1016/j.ijbiomac.2018.04.067.